NASA Technical Memorandum 106620
AIAA–94–1869

Icing Test Results on an Advanced Two-Dimensional High-Lift Multi-Element Airfoil

Jaiwon Shin
Lewis Research Center
Cleveland, Ohio

Peter Wilcox and Vincent Chin
McDonnell Douglas Aerospace
Long Beach, California

and

David Sheldon
Lewis Research Center
Cleveland, Ohio

Prepared for the
12th Applied Aerodynamics Conference
sponsored by the American Institute of Aeronautics and Astronautics
Colorado Springs, Colorado, June 20-23, 1994

National Aeronautics and
Space Administration

ICING TEST RESULTS ON AN ADVANCED TWO-DIMENSIONAL HIGH-LIFT MULTI-ELEMENT AIRFOIL

Jaiwon Shin*
National Aeronautics and Space Administration
Lewis Research Center
Cleveland, Ohio 44135

Peter Wilcox
Vincent Chin
McDonnell Douglas Aerospace
Long Beach, California 90846

David Sheldon
National Aeronautics and Space Administration
Lewis Research Center
Cleveland, Ohio 44135

Abstract

An experimental study has been conducted to investigate ice accretions on a high-lift, multi-element airfoil in the Icing Research Tunnel at the NASA Lewis Research Center. The airfoil is representative of an advanced transport wing design. The experimental work was conducted as part of a cooperative program between McDonnell Douglas Aerospace and the NASA Lewis Research Center to improve current understanding of ice accretion characteristics on the multi-element airfoil. The experimental effort also provided ice shapes for future aerodynamic tests at flight Reynolds numbers to ascertain high-lift performance effects. Ice shapes documented for a landing configuration over a variety of icing conditions are presented along with analyses.

Nomenclature

c	Stowed airfoil chord length, inch
t	Ice accretion time, minutes
T_s	Static air temperature, °F
T_t	Total air temperature, °F
V	Airspeed, mph
x	Chordwise axis
y	Axis normal to the x-axis
α	Angle-of-attack, degree
LWC	Liquid water content
MVD	Median volume droplet diameter

Introduction

High lift devices have been in use for many years. With changes in financial requirements in the airline industry, aircraft manufacturers have been working to simplify the design and increase lift/drag ratio. This has led to super critical wing designs with fewer number of high lift devices; typically a slat, and a large-chord single-segment flap. The development work of such an airfoil has been carried out by McDonnell Douglas Aerospace (MDA) in the Low Turbulence Pressure Tunnel (LTPT) at the NASA Langley Research Center.[1-4] This advanced high lift wing design is based on highly optimized gap and overhang settings, which has very little tolerance for contamination. This high sensitivity makes environmental contamination a very important issue, particularly contamination due to ice accretions. In order to understand the effects of ice accretions on the advanced high-lift airfoil aerodynamics, it is essential to test the airfoil under icing conditions that the airfoil would encounter in flight. To date, there has not been any experimental ice shape data available for this type of advanced three-element airfoil.

Prediction of the flow field around a multi-element airfoil is quite a challenging task due to the complexities associated with merging shear layers and multiple separations. Over the past few years, the viscous flow calculation capability over multi-element airfoils has seen steady improvement.[5-7] Results from the tests conducted in the LTPT [1-4] provided benchmark databases for the development of these methods. However, these calculation methods are all for clean airfoils without any consideration of surface contamination. Although flow calculation with surface contamination needs further development, the capability to predict ice shapes on multi-element airfoils has been developed.[8,9] However, further development of these ice accretion codes has been slow because of a lack of experimental ice shape data for multi-element airfoils.

The most comprehensive icing data to date on multi-element airfoils is from the test conducted in the Icing Research Tunnel (IRT) by Potapczuk, et al.[10] using a Boeing 737 two-dimensional wing section model. The test results provided ice shapes on four different configurations including the cruise configuration and flap settings with deflection angles of up to 15 degrees. Since the computational capability for ice accretions on multi-element airfoils was not developed at the time of the test, the major portion of this test was devoted

*Member AIAA

to the cruise configuration to acquire validation data for single element ice accretion codes. The advanced design developed by MDA resulted in a highly optimized gap between the main element and the flap with a larger deflection angle for the landing configuration. The multi-element ice accretion codes currently available have not been tested against this kind of highly optimized configuration because there was no data available. Therefore, a database focused more on the landing and takeoff configurations was in demand to assess the accuracy of multi-element ice accretion codes.

The objective of this test was threefold: (1) to acquire ice accretion data on a high-lift, multi-element airfoil for various configurations including the landing configuration for CFD validation and planned future aerodynamic performance tests, (2) to investigate susceptibility of ice build-up on flaps of an advanced multi-element airfoil with optimized flap gaps, and (3) to investigate effects of an anti-iced slat on ice accretions on the downstream elements. In this paper, detailed ice shape results will be presented along with surface pressure distributions of the clean airfoil for a landing configuration.

Douglas/NASA Lewis/NASA Langley Advanced High-Lift Multi-Element Airfoil Program

The cooperative program between McDonnell Douglas Aerospace and the NASA Lewis Research Center was established in 1993 to improve the understanding of ice accretion effects on multi-element airfoils. Multi-year icing tests were planned. These icing tests are part of a comprehensive development effort for an advanced high-lift, multi-element airfoil by MDA, which started a few years ago by testing several airfoil configurations and gap settings in the NASA Langley LTPT.

During the LTPT tests, it was found that maximum lift results were very much dependent on the Reynolds number, suggesting that results obtained at low Reynolds numbers can be misleading.[11] Based on these results, investigators recommended that aerodynamic testing of high-lift, multi-element airfoils be conducted in facilities that can provide flight Reynolds numbers such as the NASA Langley LTPT. For this reason, it was decided that ice shapes would be obtained in an icing tunnel, then separate aerodynamic testing would be conducted in the LTPT to study aerodynamic penalties due to ice accretions on multi-element airfoils.

Because of its unique capability in simulating natural icing conditions and its large test section, the IRT was chosen as the ideal facility to obtain necessary ice shapes for future aerodynamic tests. Ice accretion does not have to be obtained at a flight Reynolds number as long as Mach number is matched because ice accretion is primarily a near leading edge phenomenon and the boundary layer is thin at the leading edge. Therefore, use of the ice shapes obtained at low Reynolds numbers in the IRT is valid. In order to provide model similitude, the current airfoil is scaled identical to the airfoil that has been tested extensively at the LTPT for gap and overhang optimization at high Reynolds numbers and Mach numbers.[1] A test is planned in the LTPT in September of 1994 to investigate aerodynamic effects of ice accretions on high-lift aerodynamics using ice shapes obtained from the current IRT test.

Description of Test

Icing Research Tunnel

The NASA IRT is a closed-loop refrigerated wind tunnel. A 5000 hp fan provides airspeeds up to 300 mph. The refrigeration heat exchanger can control the air temperature from ambient temperature to −20 °F. The spray nozzles provide droplet sizes from approximately 15 to 40 μm median volume droplet diameters (MVD) with liquid water contents (LWC) ranging from 0.3 to 3.0 g/m^3. The test section of the tunnel is 6 ft high and 9 ft wide. Figure 1 shows the schematic view of the IRT.

Model

The model is a two-dimensional multi-element airfoil model designed and fabricated specifically for vertical installation in the IRT. The current model can be assembled in a number of different three-element configurations. The cruise wing configuration has a nominal span of 71.75 in. and a chord of 36 in. For this test entry, however, no accommodations were provided for assembling the model in the cruise configuration. Model parts available for testing include a slat with an anti-ice system, a main element assembly, and flap components which can be assembled into four different configurations. A total of 128 static pressure orifices are available for hookup at one time for the three-element model. Pressure orifice rows include a single row at midspan and spanwise rows on the upper surface of the slat and flap elements only.

The high-lift components of the model are rigged to the main element each with a set of four one-piece steel brackets. These brackets set a baseline combination of deflection, overhang, and gap. Deflection is defined as the angle between the main element wing reference plane (WRP) and the deflected component WRP. Overhang is defined as the horizontal distance (i.e., parallel to the WRP) between the trailing edge of one element and the leading edge of the downstream element. Gap is defined as the minimum distance between the trailing edge of an element and the downstream element. Gap variation through vertical translation only is obtained by installing or removing a set of four constant thickness 0.09 in. thick shims between the brackets and the main element. Two sets of slat brackets and three sets of flap brackets are available for this entry.

Slat. The leading edge slat is a conventional type slat fabricated of aluminum. Installed internally in the hollow slat is a hot air anti-ice system consisting of a 0.5 in. outside diameter porous steel pipe manifold sealed at its downstream end. A source external to the test section provides hot air into

the manifold up to a maximum of 300 °F to maintain approximate slat surface temperatures of 100 °F in the slat leading edge region and above 32 °F over the remaining external surface of the slat. Sets of brackets are available to support and rig the slat to the main element at deflections of 20 and 30 degrees and a set of 0.090 in. shims is provided to vary the vertical height of the slat with respect to the main element. The slat has 35 chordwise and 6 spanwise static pressure orifices, and 4 thermocouples installed in the leading edge.

Wing Main Element. The aluminum main element is comprised of a main spar with removable Wing-Under-Slat-Surface (WUSS), main spar, spoiler, and Bent-Up-Trailing-Edge (BUTE) components. The wing spar is designed to accommodate the installation of support brackets for the high-lift components. Allowances have also been made for the exit of pressure tubing (flap and slat) and thermocouple leads (slat only) from the lower surface side of the model through the lower tunnel turntable with minimal interference to the local freestream. The main element has 42 chordwise and no spanwise static pressure orifices.

Flap. An aluminum flap assembly was tested during the entry. The configuration is a two-piece assembly comprised of a forward component and an aft component. The forward section represents the VF90B (nonproprietary conventional leading edge), while aft section represents a stowed auxiliary flap with a conventional trailing edge (AUX). The flap assembly has 33 chordwise pressure orifices and a total of 12 spanwise pressure orifices in two rows; one in the forward and the other in the aft component.

IRT Facility Measurement Systems

Electronic Scanning Pressure System. The model surface pressures were measured with the IRT facility electronic scanning system (ESP). The ESP system offers a transducer per measurement to produce high data rates for multiple pressure measurements with errors no greater than ±0.10 percent of full scale. This is accomplished by a three point pressure calibration to all port transducers. Each calibration pressure is measured with a precision digital quartz transducer. The standard calibration interval is every 400 cycles (approximately 15 min). The reference pressure to the ESP system is located outside of the tunnel balance chamber due to static pressure changes within the chamber. The balance chamber which is vented to the test section sees the local velocity static pressure.

The ESP system capacity was expanded to include six 32-port (±5 psid) modules for a total of 192 pressure channels for this test. A check pressure applied to port 1 of each module was used to initiate ESP transducer calibration when its level deviated beyond a threshold of ±0.05 psi.

Facility Heated Bleed Air System. The facility heated bleed air system supplied the hot air to the model slat anti-icing system. The high pressure air is supplied by the Lewis Central Air System at 120 psig and up to one lbm/sec. The mass flow is limited due to the piping size into the facility. The air is heated by one or both facility support systems, a natural gas burner and/or a 45 kW electric heat exchanger. The maximum temperature if both systems are in use is 900 °F. The model slat anti-icing system was supported by only the electric heat exchanger. The heated bleed air mass flow was measured by a subsonic venturi having a flow range of 0.1 to 0.6 lbm/sec.

Test Method

The icing test was conducted to obtain mainly two types of icing data; ice shape data for scaled icing conditions (scaling runs) and ice shape data for numerical code validation (CFD runs). The scaling method used in this test is the method of Ruff.[12] If geometrically scaled ice shapes are to be accreted on a sub-scale model, several parameters must be held constant. Ruff's method holds droplet trajectories and accumulation parameter constant between the full scale and sub scale. In addition, energy transfer is matched between the two cases by holding freezing fraction, air and droplet energy transfer terms constant. The full scale conditions chosen for this test are representative of a continuous icing condition. The full scale conditions are LWC of 0.3 g/m^3, icing time of 24 min, MVD of 25 μm, and static temperature of 24 °F. These values were chosen as appropriate values from the section of the Federal Aviation Regulations (FAR) containing the envelopes of icing conditions (FAR part 25). The icing conditions used for the scaling runs were repeated for anti-icing runs to study effects of the anti-iced slat on the ice accretions of the downstream elements. During the anti-icing runs, the slat was heated to about 100 °F, which kept the surface completely free of ice. CFD runs were made to generate a database for code validation at takeoff and landing configurations for a variety of icing conditions.

Prior to testing each configuration for icing, surface pressure measurements were made with the clean airfoil at various angles-of-attack. During the pressure measurement, the airfoil was rotated from –4 to 16 degrees at a 4 degree increment. The airfoil was not tested at angles higher than 16 degrees because target airspeeds could not be obtained due to the blockage generated by the airfoil.

To measure the contour of the accreted ice on each element, a simple tracing technique was used. After completion of each icing run, slices were made in the ice with heated aluminum plates at each measurement location. Once all the ice had been removed at each location, a cardboard template cut to the shape of the airfoil surface was inserted into the cut. Using a sharp pencil and insuring that the side of the lead was kept in contact with the ice, the accreted ice shape was traced onto the cardboard template. Ice shape tracings were taken at four spanwise locations for all primary runs, while tracings were only taken at the middle two locations for repeat runs.

To improve the accuracy of this technique, two precision items were used. First, the slices in the ice were made with

aluminum plates which had been wire cut to the exact coordinates of the airfoil. This helped to assure that the ice was completely melted in each slice. Second, the tracing templates were cut by precision rule die. The resulting tracing templates were uniform and true to the airfoil surface. In addition, two reference points were cut into the tracing templates by the die. These reference points allowed exact positioning of the measured ice shape in relation to the airfoil after the tracing had been digitized and stored onto a computer disk.

A typical procedure for an icing run is as follows.

1. The target airspeed and total temperature were set.
2. The spray system was configured for the desired MVD and LWC.
3. The spray system was turned on for the desired spray time.
4. The tunnel was brought down to fan idle for ice shape tracings and photographs.
5. The airfoil was then cleaned and the tunnel conditions set for the next data point.

Test Conditions

Test conditions for the icing test were grouped into two categories for the reason described in the previous section: (1) scaling runs with the landing and takeoff configurations, and (2) CFD validation runs with the landing configuration. For scaling runs, all four flap configurations were tested for the same icing condition at 114 mph, 16.8 °F (total temperature), a LWC of 0.66 g/m^3, a MVD of 14 μm for a 4 minute spray. CFD validation runs were tested with varying airspeeds (150 and 198 mph), total temperatures (30, 27, 17, and 14 °F), LWCs (0.6 and 1.2 g/m^3), and MVDs (20 and 25 μm). Spray time was fixed at 6 minutes. Icing runs were made at three different angles-of-attack: 0, 4, and 8 degrees. Table I lists the icing conditions for the test points presented in this paper.

Results and Discussions

A total of 129 icing runs were completed and 10 angle-of-attack sweep runs were made during the test. Detailed ice shape results are presented in this section with the flap setting of VF90B+AUX for the landing configuration which had a flap deflection angle of 30 degrees. Chordwise and spanwise pressure distributions for the clean airfoil are also presented.

Surface Pressure Distributions for the Clean Airfoil

In order to evaluate the aerodynamic performance of the "clean" multi-element airfoil configuration, a total of 128 static pressure orifices were installed in the model components and hooked up to the IRT ESP system. These orifices were distributed in a single chordwise row at model midspan on all three elements, and also in spanwise rows located on the upper surface of the slat (5 percent stowed chord) and flap (74 and 100 percent stowed chord). Trapezoidal integration (nondimensionalized by stowed chord) of the chordwise pressures was performed to evaluate the component section lift distributions of the model. Observation of the spanwise pressure distributions provided an assessment of the level of two-dimensionality of the flow about the model.

Figure 3 presents the pressure integrated section lift characteristics of the three-element model configuration as a function of model angle-of-attack. As can be seen, the trends are representative of typical multi-element, high-lift characteristics. As angle-of-attack is increased, the slat and main element components load up while the flap unloads. This characteristic is a result of a downwash effect on the flap caused by the increased circulation about the forward elements.

Figure 4 shows a typical chordwise pressure distribution for the landing configuration at the angles-of-attack at which the ice accretion measurements were taken. The data reflects the typical characteristics of flow about a multi-element airfoil. The local re-acceleration region at approximately 16 percent chord is reflective of a model surface discontinuity, the point at which the Wing Under Slat Surface (WUSS) transitions to the main wing geometry. The flow over the upper surface of the flap remains fully attached for the two angle-of-attack conditions shown. The high aspect ratio (2.0) of the model does help to minimize the influence of the tunnel wall boundary layers on the chordwise pressure located at midspan.

Figure 5 presents a typical spanwise pressure distribution for the multi-element model at a 4 degree of angle-of-attack. As expected, there is a slight degree of three-dimensionality in the flow, especially near the leading edge of the flap. This condition can be attributed to the existence of a region of separated flow located upstream of the flap in the flap well cove. Near the tunnel walls (i.e., tunnel floor/ceiling in the IRT), this separated region is worsened due to the lack of wall boundary layer control. Consequently, the effect of this separated region, coupled with the adverse pressure gradient downstream of the flap pressure peak, causes the three-dimensional nature of the flow at the ends of the flap. It should be noted that, in the vicinity of the spanwise region of the model where ice accretion measurements were obtained (35 to 65 percent span), the two-dimensionality of the flow over all three elements was satisfactory.

Ice Shape Results

Ice shape tracings were made at four spanwise stations on each element to document spanwise variations. Ice shape tracings made at the two middle stations are presented herein because the icing cloud is most uniform in the center of the test section.

Repeatability of ice shapes in the IRT has been documented previously on a single element airfoil.[13] All CFD validation runs have repeat runs to ensure that repeatable ice shapes were obtained. Repeatability of rime ice shapes was excellent and the repeatability of glaze ice was good. This

result is consistent with the result found in ref. 13. Figures 6 and 7 show comparison of glaze ice shapes obtained from two separate runs for the same icing condition. All ice shape tracings are shown in stowed, nondimensional coordinates. Major features of the ice shape and the amount of ice compare well on all three elements. This kind of repeatability is typical for all the data obtained during the test.

Scaling Runs. Scaling runs were made with one common icing condition for three angles-of-attack; 0, 4, and 8 degrees. The icing condition was for V = 114 mph, T_t = 16.8 °F, LWC = 0.66 g/m^3, MVD = 14 μm, and t = 4 min. This icing condition produced rime ice with very little spanwise variation.

Figure 8 shows ice shapes traced at the slat, main element, flap leading edge and flap trailing edge for 0 degree of angle-of-attack. Figures 9 and 10 show ice shapes for 4 and 8 degrees of angle-of-attack respectively. Icing limits on the slat leading edge show a big shift as the AOA changes, however icing limits on the main element and the flap leading edge are far less sensitive to the AOA changes. The stagnation line was visible on the ice accretion on the main element at about x/c = 0.09 for a = 0 degrees, and the location of the stagnation line moved further downstream as the AOA increased. Ice was accreted on the entire lower surface of the flap at all three angles-of-attack. Less ice accretion (or thinner ice accretion) is observed on the main element as the angle-of-attack increases. However, more ice accretion (or thicker ice accretion) is observed on the flap as the angle-of-attack increases.

The same icing condition was used to study the effect of slat anti-icing on the ice accretion of the downstream elements. Figures 11 to 13 show the results for α = 0, 4, and 8 degrees respectively. The slat surface was heated with hot air to about 100 °F during this phase of the test as described in the previous section. The ice shape results show no noticeable effects of slat anti-icing on the trends of ice accretions on the main element and the flap as shown in figures 8 to 10. Icing limits on the main element and the flap moved very little, and less ice accretion on the main element and more ice accretion on the flap are observed as the angle-of-attack increases.

CFD Runs. Icing conditions for the CFD runs were devised using two airspeeds, two static temperatures, two LWCs, two MVDs, and two angles-of-attack in order to capture effects of various icing parameters on the ice accretion. The results are presented in several categories in terms of icing parameters for temperature, airspeed, LWC, and MVD. A base data point was selected for comparisons. The icing condition for the base point is α = 4 degrees, V = 198 mph, T_t = 30 °F, LWC = 0.6 g/m^3, MVD = 20 μm, and t = 6 min. This base condition represents a typical glaze ice accretion and the ice shape tracings are shown in figure 6.

Temperature Effect: For this category, all icing parameters remained constant except the temperature. Two total temperatures compared here are 30 °F and 17 °F. Figure 6 shows ice shapes on all three elements for 30 °F and figure14 for 17 °F. Icing limits on all three elements between the two temperatures are similar with the biggest difference found on the slat. Slat ice accretion at 30 °F displays distinct upper and lower horns which are characteristic of typical glaze ice accretion. Slat ice accretion at 17 °F shows a smooth extension of the leading edge contour which is characteristic of typical rime ice accretion. Difference in ice accretions on the main element and the flap leading edge between the two temperatures is small compared with the difference shown with the slat ice accretions. However, it is observed that horn development is apparent on the main element and the flap leading edge at 30 °F.

Spanwise variation in the ice shape is greater at the warmer temperature as expected. Ice accretion on the main element extends chordwise past the metal template at both temperatures. Ice accretion was never grown into the gaps between the elements at either temperatures. Ice accreted on the entire lower surface of the flap for both temperatures with much thicker ice accretion at the trailing edge. Ice accretion on the lower surface of the flap at 17 °F was feathery type and very brittle. These feathers tended to break off while tracings were made, which makes the thickness of ice appear thinner compared with the glaze ice case.

Ice shapes at α = 8 degrees show the same features and trends as the results at 4 degrees with the only major difference being a shift of the slat leading edge icing limits. This observation was true for other icing parameter results as well. Therefore, the results at 4 degrees of angle-of-attack are only presented herein.

Airspeed Effect: The two airspeeds tested were 198 mph and 150 mph. Since all other icing parameters were identical, the net change is a higher water loading with the higher airspeed, resulting in more ice accretion, as shown in a comparison between figures 6 and 15. Figure 15 shows ice accretions at 150 mph. Slat leading edge ice at the higher airspeed shows more prominent horn development with a bigger ice accretion. Features of the ice accretion on the main element and the flap look very similar between the two airspeeds, especially the pattern of the horn development. It appears that ice accretion features are not affected much on the main element and the flap by the change in airspeed.

LWC Effect: For this study, the LWC is doubled from the base condition (fig. 6) to 1.2 g/m^3. Due to much higher water loading, water flowed further back on the surface before starting to freeze. This runback resulted in much bigger horn growth at all three elements at the higher LWC as shown in figure16. It is noteworthy that the locations of the horn development remain fairly constant on the main element and the flap between the two LWCs. Again the entire lower surface of the flap was covered with ice and the ice accretion at the trailing edge of the flap at the higher LWC was significant.

MVD Effect: Two drop sizes were used to study the MVD effect; 20 and 25 μm. Although, the spread in the MVD was small, the slat ice showed a significant difference between the two drop sizes as shown in figures 6 and 17. Figure 17 shows ice accretion tracings with the MVD of 25 μm. Both upper and lower icing limits moved further downstream with the bigger MVD. Ice accretion on the other two elements show very little difference between the two drop sizes suggesting their droplet trajectories were not affected much by the change of the MVD.

Summary

Ice shape tracing results from the IRT test on a high-lift, multi-element airfoil have been presented. This database serves two important purposes: 1) to gain a better understanding of ice accretion on the high-lift, multi-element airfoil, and 2) to build a database for CFD validation. Several noteworthy findings are listed below.

1. Slat ice accretion was sensitive to the change in icing parameters much like the leading edge of a single element airfoil. However, ice accretions on the main element and the flap were much less sensitive to the change in icing parameters.

2. Slat anti-icing had very little effect on ice accretions on the downstream elements for the icing conditions tested.

3. For all icing conditions tested, the entire lower surface of the flap accreted ice. Ice accretion at the trailing edge of the flap was significant for most cases.

4. Gaps between the elements were never contaminated for the icing conditions and flap settings that were tested. Ice generally accreted away from the gap preventing the gap from being filled by the ice accretion.

These results are an important step in determining the impact of ice accretion on high-lift systems. Follow-on testing will be required to determine performance effects. The ultimate aim of this research is to determine the effects of ice accretion on a realistic three-dimensional high-lift system. This will require ice accretion and performance testing of a three-dimensional high-lift system. More icing tests are also planned in the IRT to acquire more complete database for the landing and takeoff configurations with various flap settings.

Acknowledgment

The authors sincerely appreciate the support provided by the IRT staff for making the test successful and very productive. Tammy Langhals of NYMA, Inc. is acknowledged for her hard work in digitizing ice shape tracings. The effort provided by Steve Wells during the test and during data reduction is greatly appreciated.

References

1. Valarezo, W.O., Dominik, C.J., McGhee, R.J., Goodman, W.L., and Paschal, K.B., "Multi-Element Airfoil Optimization for Maximum Lift at High Reynolds Numbers," AIAA Paper 91-3332, September, 1991.
2. Valarezo, W.O., Dominik, C.J., McGhee, R.J., and Goodman, W.L., "High Reynolds Number Configuration Development of a High-Lift Airfoil," AGARD Conference Proceedings 415, pp. 10-1 to 10-8, October, 1992.
3. Valarezo, W.O., Dominik, C.J., and McGhee, R.J., "Reynolds and Mach Number Effects on Multielement Airfoils," Fifth Symposium on Numerical and Physical Aspects of Aerodynamic Flows, Long Beach, January, 1992.
4. Valarezo, W.O., "High Lift Testing at High Reynolds Numbers," AIAA Paper 92-3986, July, 1992.
5. Rogers, S.E., Wiltberger, N.L., and Kwak, D., "Efficient Simulation of Incompressible Viscous Flow Over Single and Multi-Element Airfoils," AIAA Paper 92-0405, January, 1992.
6. Rogers, S.E., "Progress in High-Lift Aerodynamic Calculations," AIAA Paper 93-0194, January, 1993.
7. Anderson, W.K., and Bonhaus, D.L., "Navier-Stokes Computations and Experimental Comparisons for Multielement Airfoil Configurations," AIAA Paper 93-0645, January, 1993.
8. Chen, H.H. and Cebeci, T., "Prediction of Ice Shapes on Wings and Multielement Airfoils," AIAA Paper 94-0608.
9. Eberhardt, S., Li, W., Kim, B., Ok, H., and Taflin, D., "BUWICE - An Interactive Icing Program Applied to Multi-Element Airfoils," AIAA Paper 94-0607.
10. Potapczuk, Mark and Berkowitz, Brian, "An Experimental Investigation of Multi-Element Airfoil Ice Accretion and Resulting Performance Degradation," AIAA Paper 89-0752.
11. Lynch, F.T., Valarezo, W.O., and McGhee, R.J., "The Adverse Aerodynamic Impact of Very Small Leading Edge Ice (Roughness) Buildups on Wings and Tails," Proceedings of 68th AGARD Fluid Dynamics Panel Specialists Meeting on Effects of Adverse Weather on Aerodynamics, CP 496, December, 1991.
12. Ruff, G.A., "Analysis and Verification of the Icing Scaling Equations: Analysis and Verification," AEDC-TR-85-30, Vol.1, March, 1986.
13. Shin, J. and Bond, T. H., "Results of an Icing Test on a NACA 0012 Airfoil in the NASA Lewis Icing Research Tunnel," AIAA Paper 92-0647, January, 1992.

Table I.–ICING CONDITIONS FOR THE DATA POINTS PRESENTED IN THE PAPER

Flap Setting: VF90B + AUX
Configuration: Landing

(a) Clean Angle-of-Attack Sweep

Run No.	AOA (degree)	Total T ($^{\circ}$F)	Velocity (mph)	LWC (g/m^3)	MVD (μm)	Time (min)
26	sweep	16.8	114	NA	NA	NA

(b) Scaling Runs

Run No.	AOA (degree)	Total T ($^{\circ}$F)	Velocity (mph)	LWC (g/m^3)	MVD (μm)	Time (min)
27	0	16.8	114	0.66	14	4
28	4	〃	〃	〃	〃	〃
29	8	〃	〃	〃	〃	〃
32*	0	〃	〃	〃	〃	〃
31*	4	〃	〃	〃	〃	〃
30*	8	⋁	⋁	⋁	⋁	⋁

* Anti-icing runs

(c) CFD Validation Runs

Run No.	AOA (degree)	Total T ($^{\circ}$F)	Velocity (mph)	LWC (g/m^3)	MVD (μm)	Time (min)
33	4	30	198	0.6	20	6
34	〃	30	198	0.6	25	6
39	〃	27	150	0.6	20	6
41	〃	17	198	0.6	20	6
107	⋁	30	198	1.2	20	6

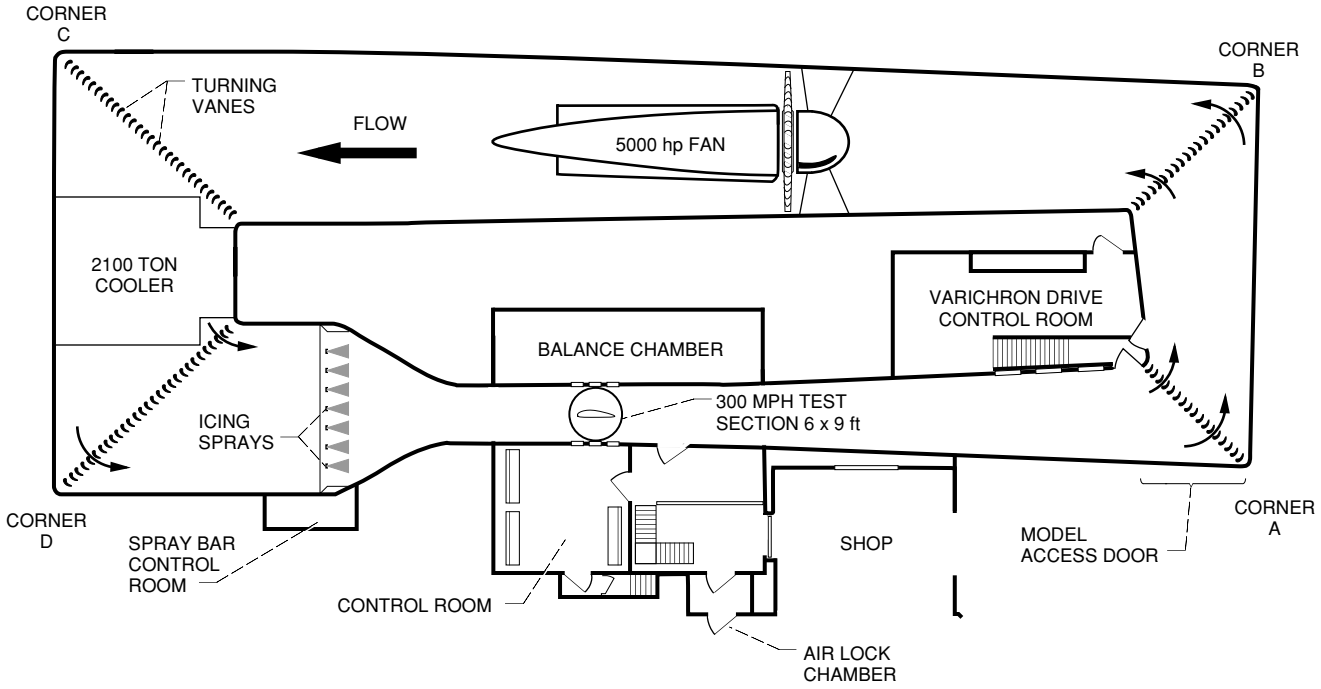

Figure 1.—Plan view of Icing Research Tunnel.

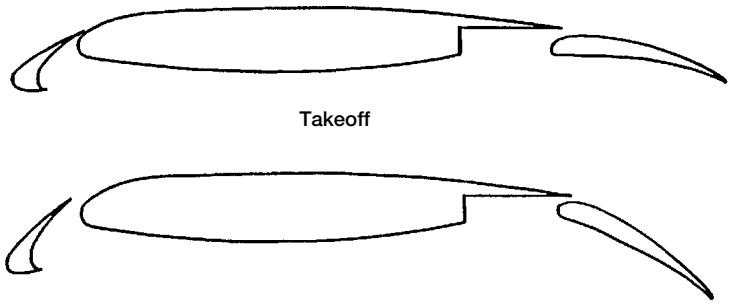

Figure 2.—High-lift model configurations.

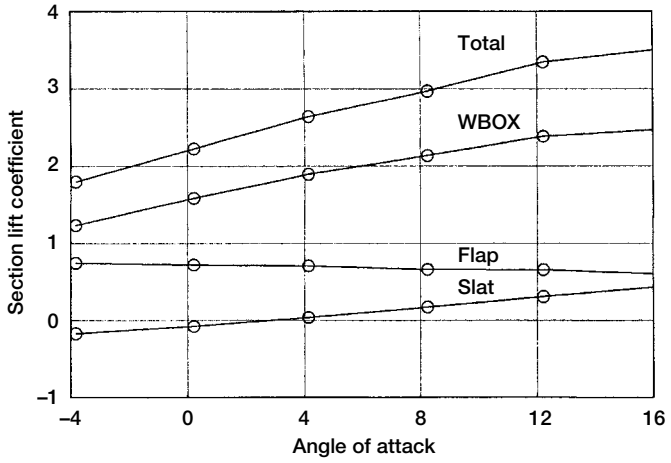

Figure 3.—Characteristics of section lift coefficient of the high-lift model.

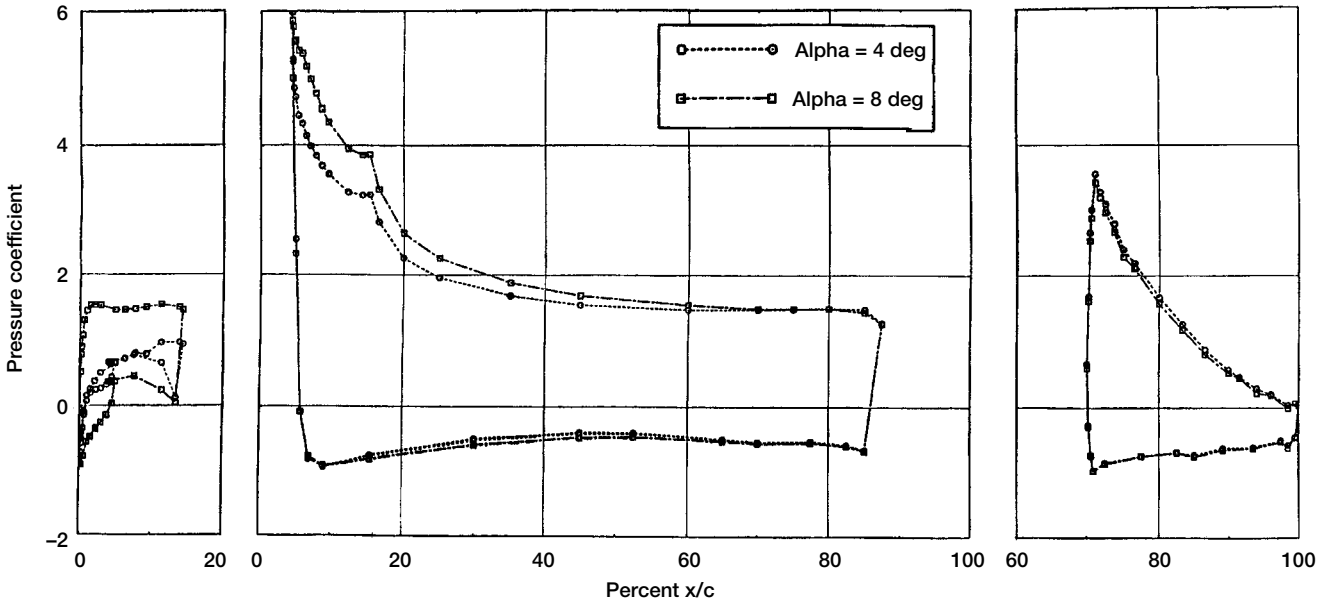

Figure 4.—Typical chordwise pressure distribution of the high-lift model.

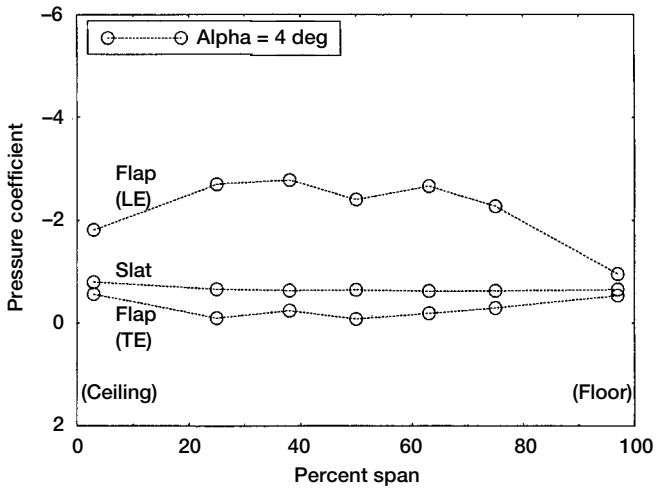

Figure 5.—Typical spanwise pressure distribution of the high-lift model.

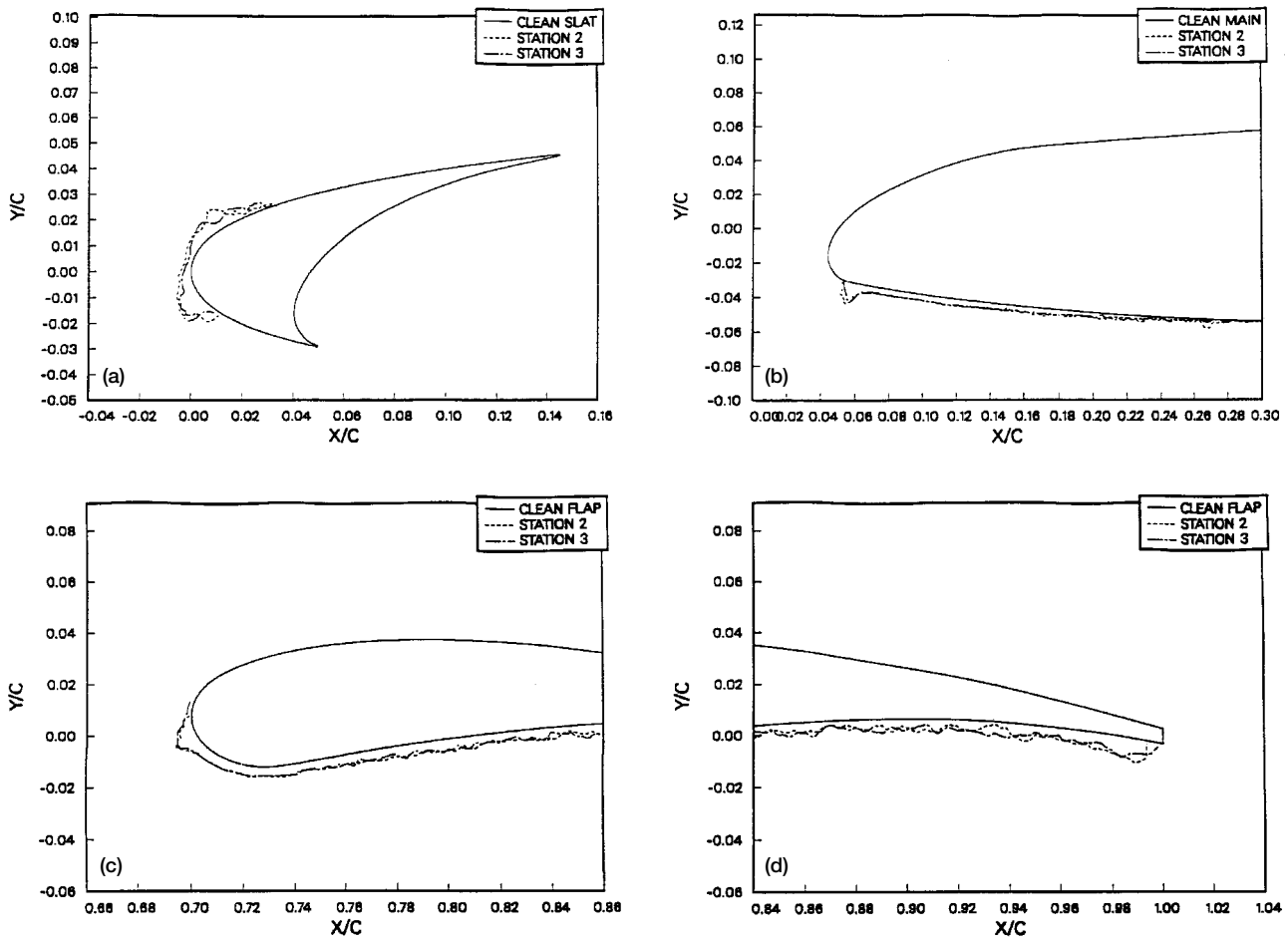

Figure 6.—Ice accretion traces for run number 33. AOA = 4°, T_t = 30 °F, V = 198 mph, LWC = 0.6 g/m^3, MVD = 20 μm, t = 6 min. (a) Slat. (b) Main element. (c) Flap leading edge. (d) Flap trailing edge.

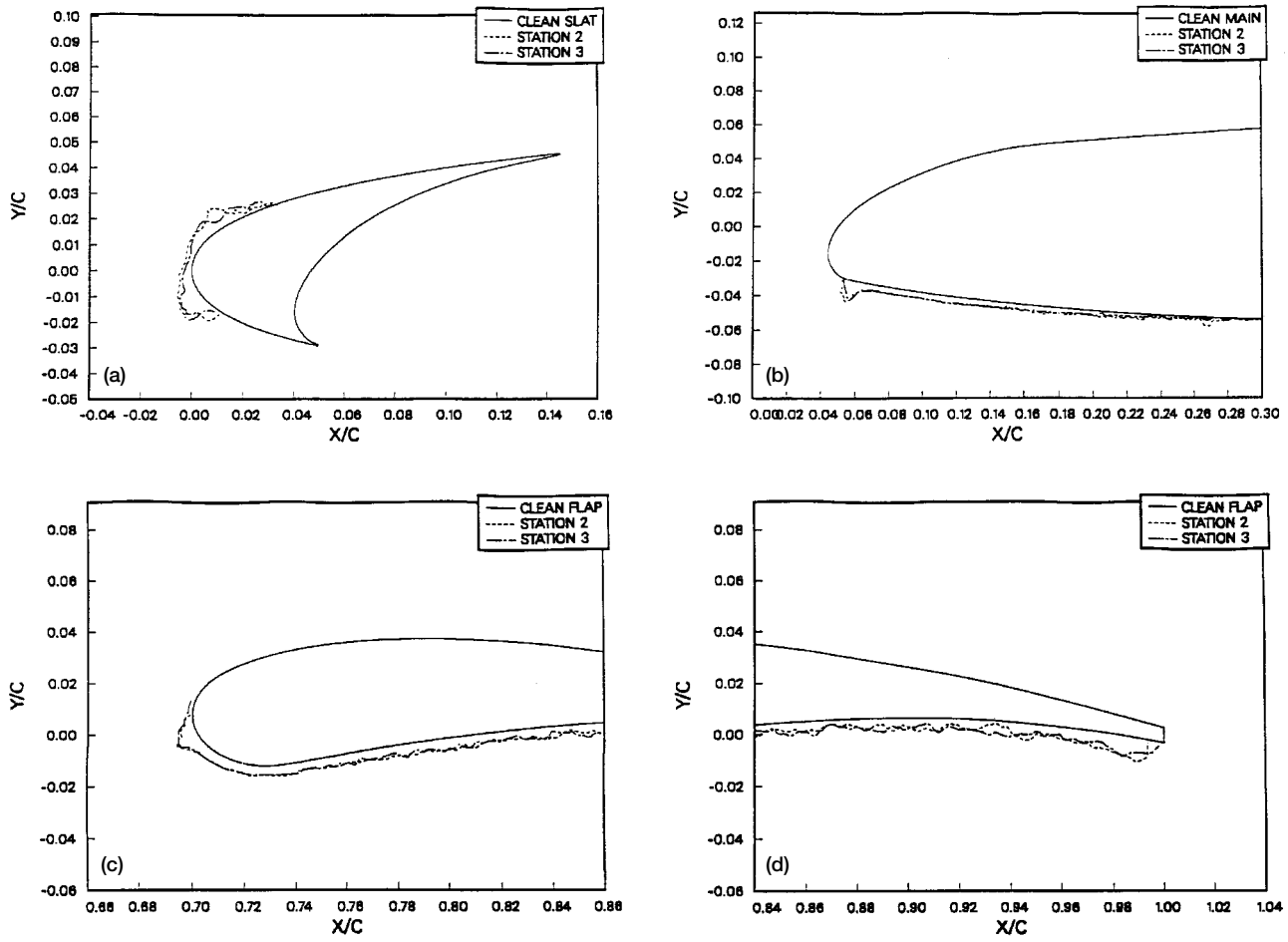

Figure 6.—Ice accretion traces for run number 33. AOA = 4°, T_t = 30 °F, V = 198 mph, LWC = 0.6 g/m^3, MVD = 20 μm, t = 6 min. (a) Slat. (b) Main element. (c) Flap leading edge. (d) Flap trailing edge.

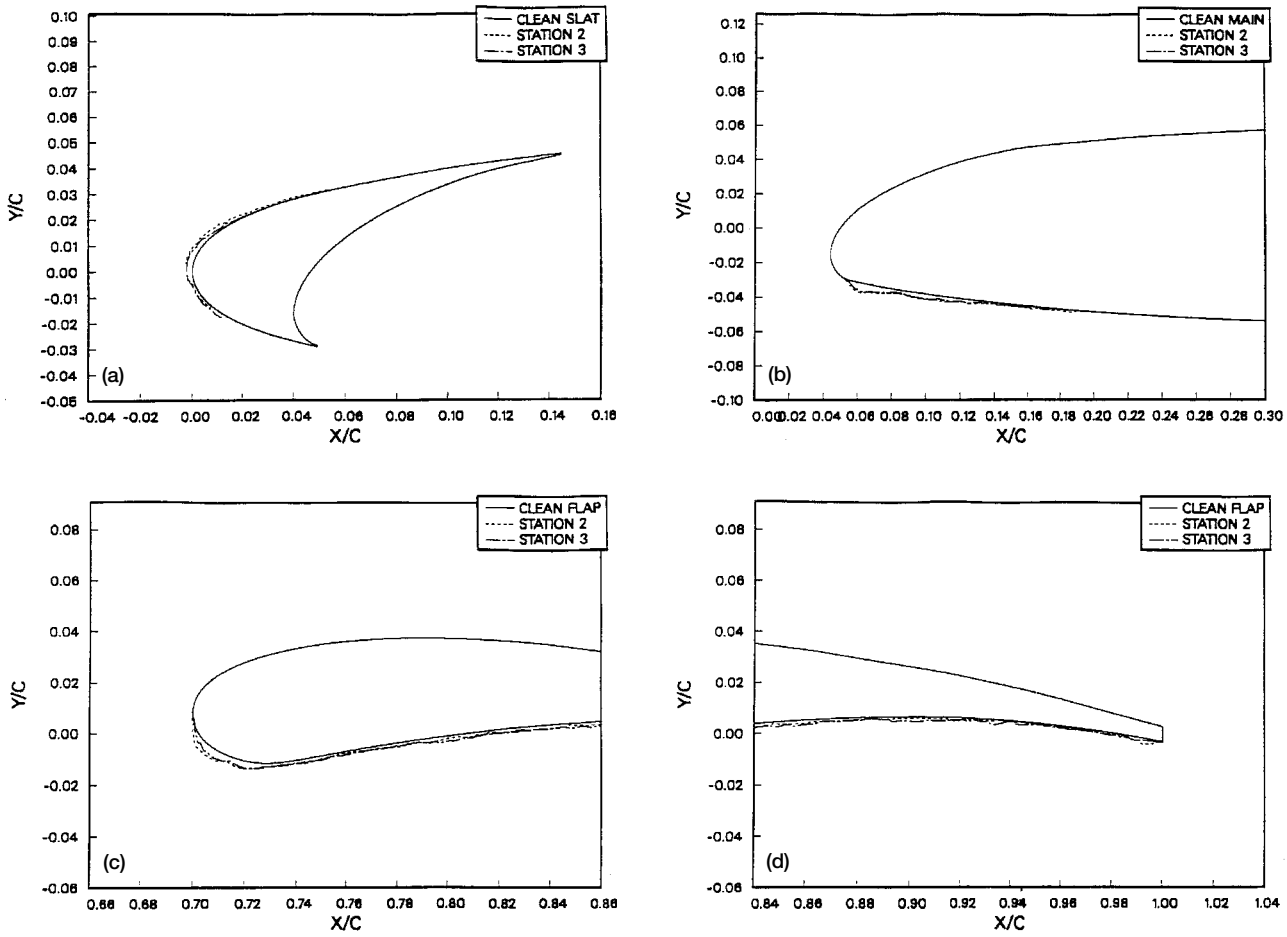

Figure 8.—Ice accretion traces for run number 27. AOA = 0°, T_t = 16.8 °F, V = 114 mph, LWC = 0.66 g/m^3, MVD = 14 μm, t = 4 min. (a) Slat. (b) Main element. (c) Flap leading edge. (d) Flap trailing edge.

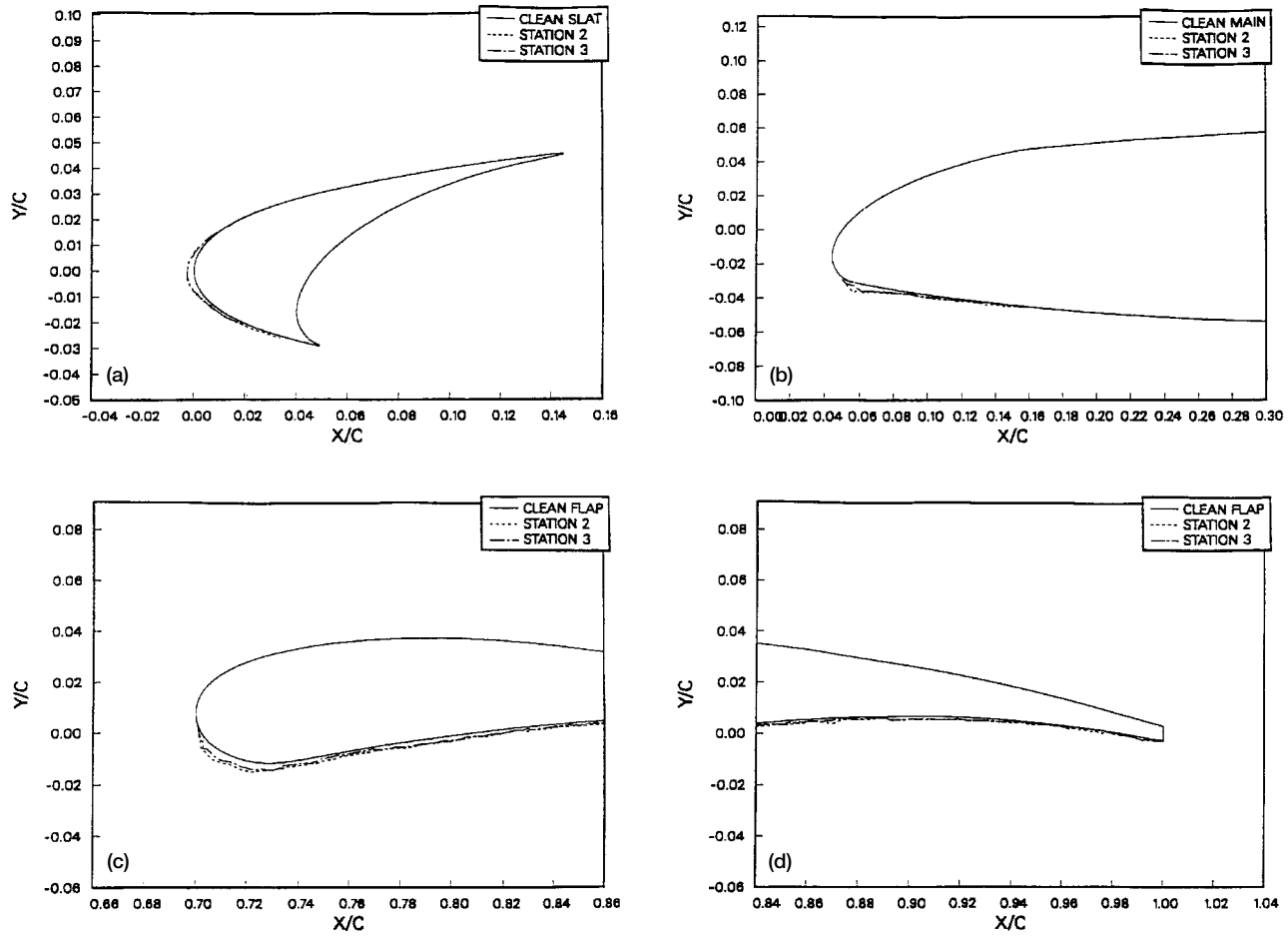

Figure 9.—Ice accretion traces for run number 28. AOA = 4°, T_t = 16.8 °F, V = 114 mph, LWC = 0.66 g/m^3, MVD = 14 μm, t = 4 min. (a) Slat. (b) Main element. (c) Flap leading edge. (d) Flap trailing edge.

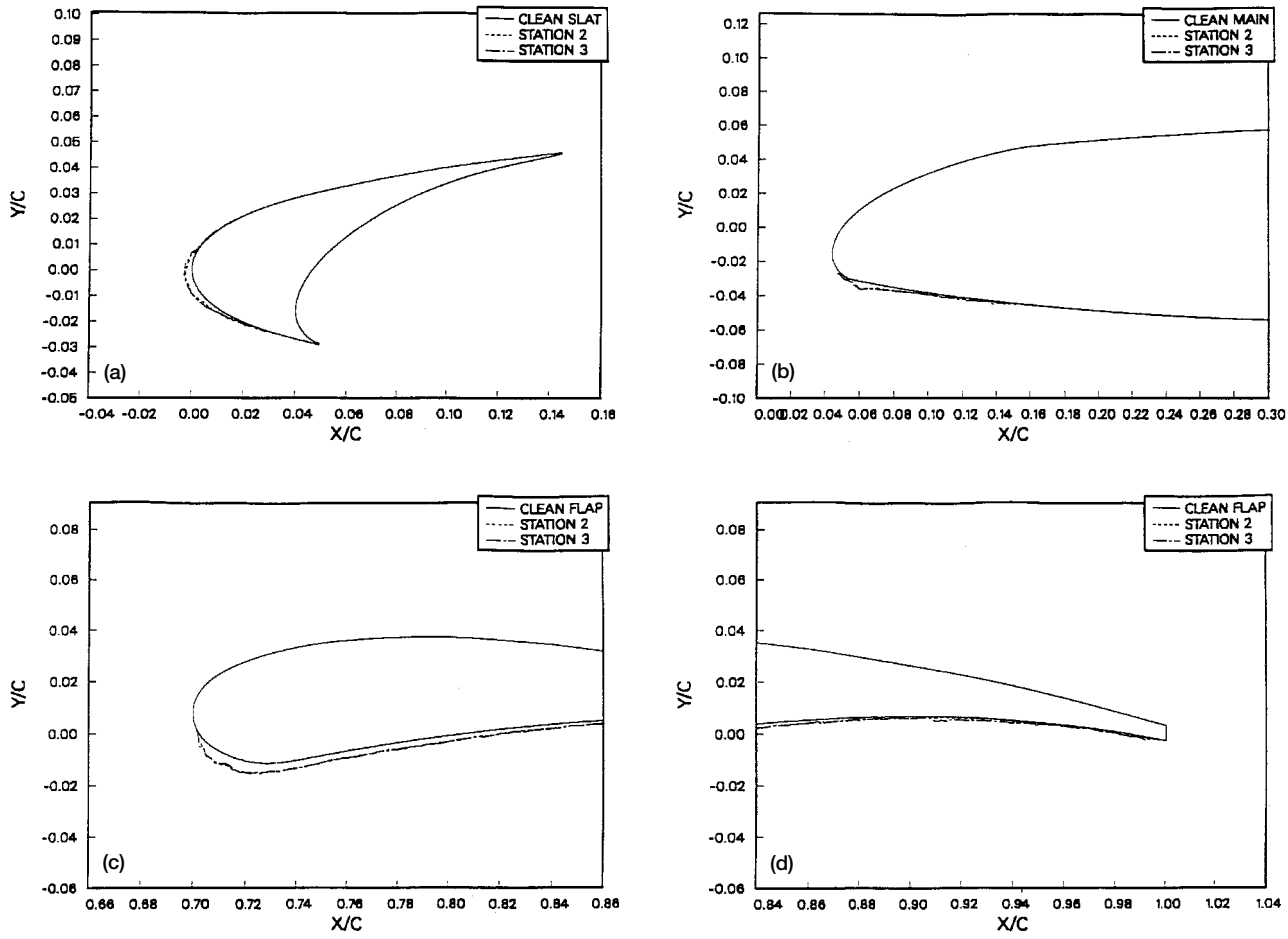

Figure 10.—Ice accretion traces for run number 29. AOA = 8°, T_t = 16.8 °F, V = 114 mph, LWC = 0.66 g/m^3, MVD = 14 μm, t = 4 min. (a) Slat. (b) Main element. (c) Flap leading edge. (d) Flap trailing edge.

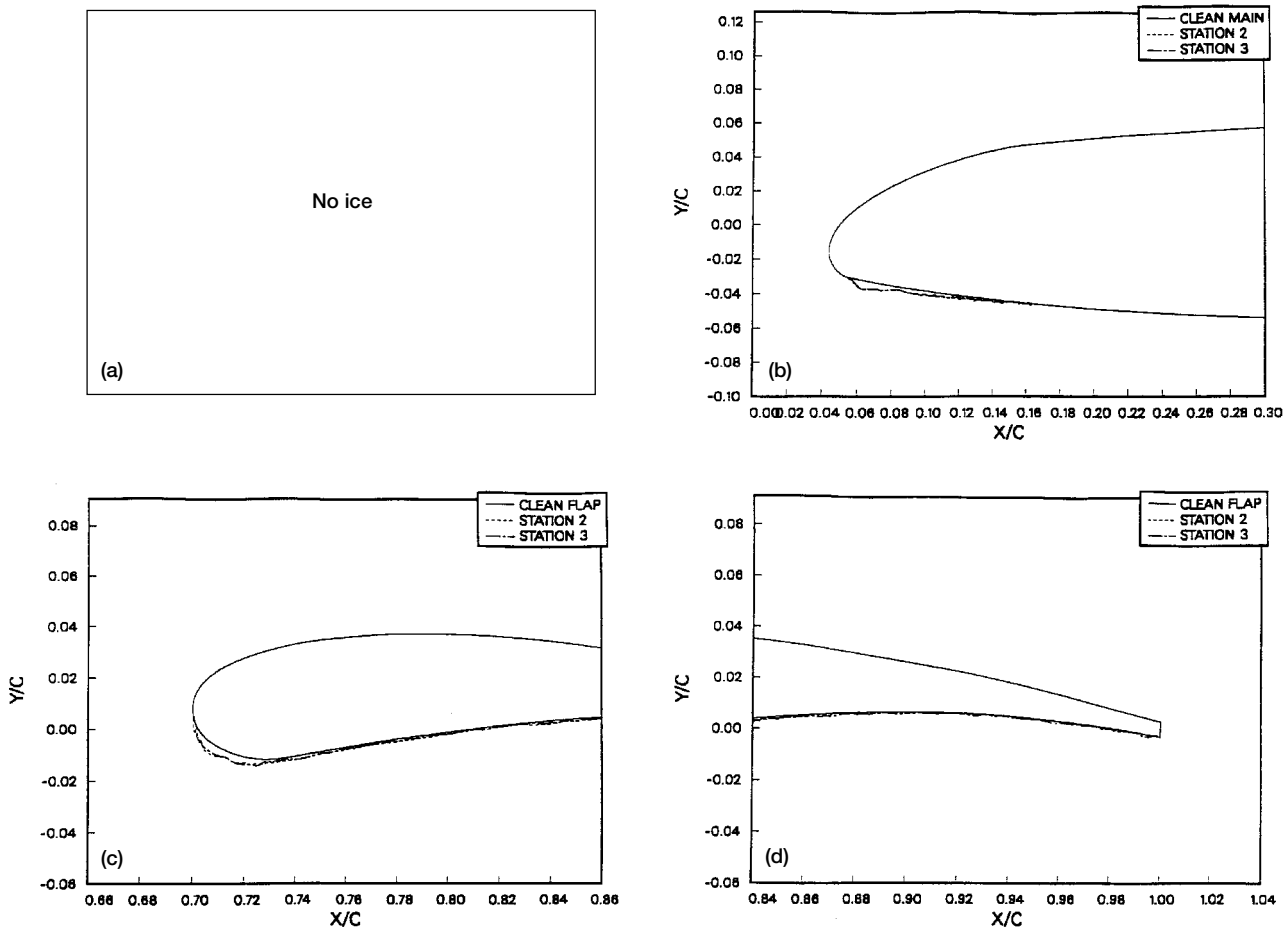

Figure 11.—Ice accretion traces for run number 32 (slat anti-icing run). AOA = 0°, T_t = 16.8 °F, V = 114 mph, LWC = 0.66 g/m^3, MVD = 14 μm, t = 4 min. (a) Slat. (b) Main element. (c) Flap leading edge. (d) Flap trailing edge.

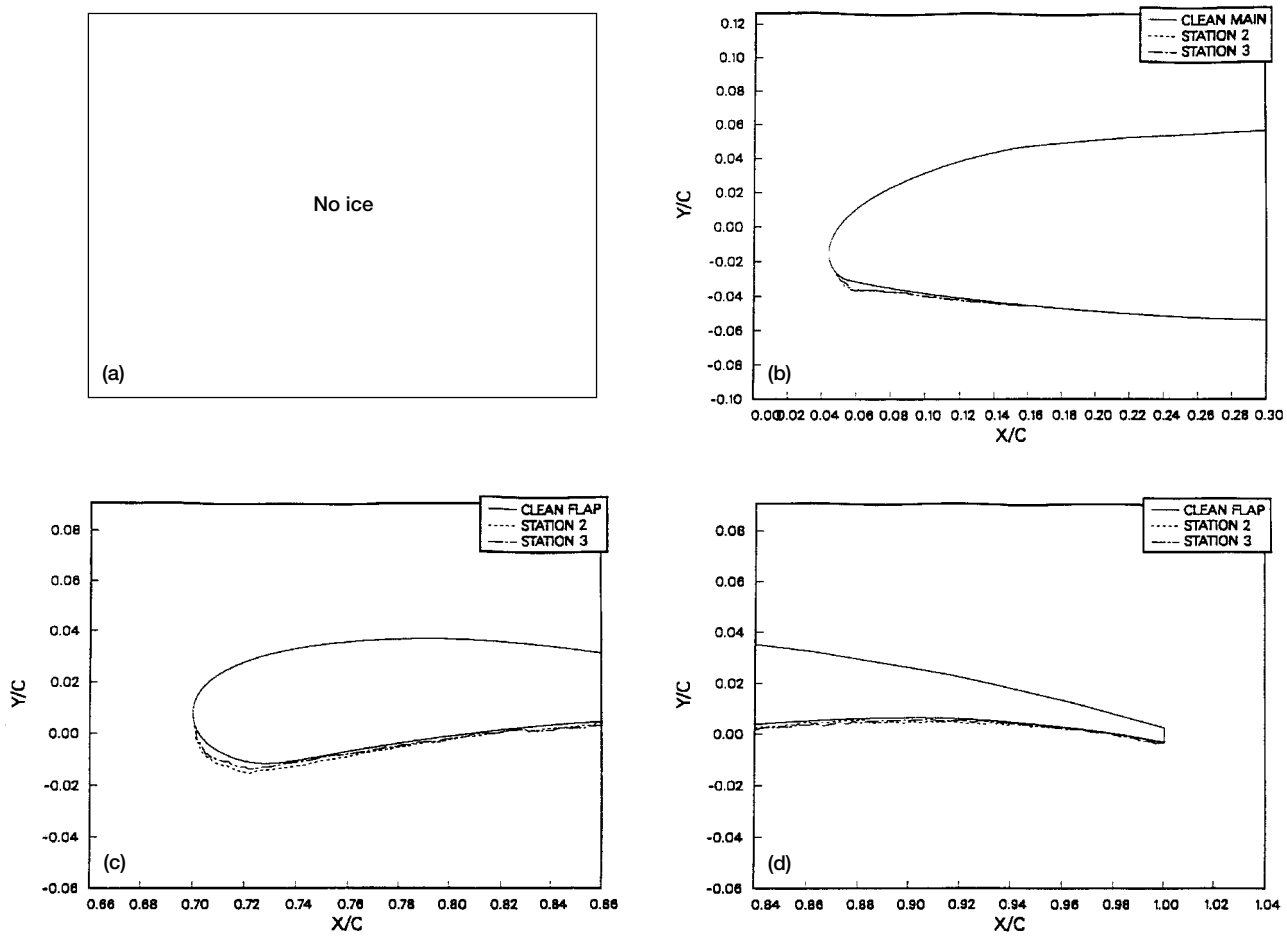

Figure 12.—Ice accretion traces for run number 31 (slat anti-icing run). AOA = 4°, T_t = 16.8 °F, V = 114 mph, LWC = 0.66 g/m^3, MVD = 14 μm, t = 4 min. (a) Slat. (b) Main element. (c) Flap leading edge. (d) Flap trailing edge.

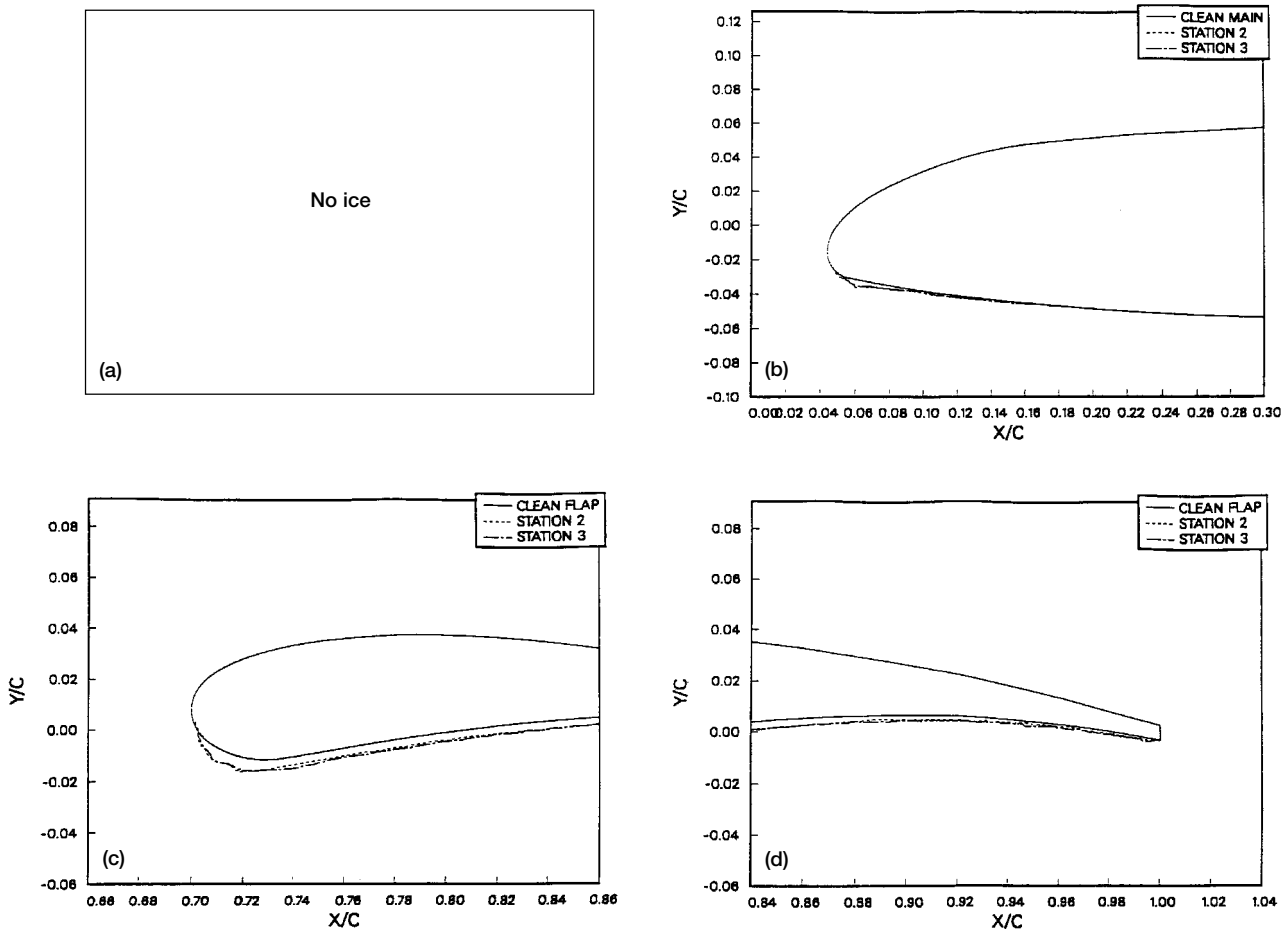

Figure 13.—Ice accretion traces for run number 30 (slat anti-icing run). AOA = 8°, T_t = 16.8 °F, V = 114 mph, LWC = 0.66 g/m^3, MVD = 14 μm, t = 4 min. (a) Slat. (b) Main element. (c) Flap leading edge. (d) Flap trailing edge.

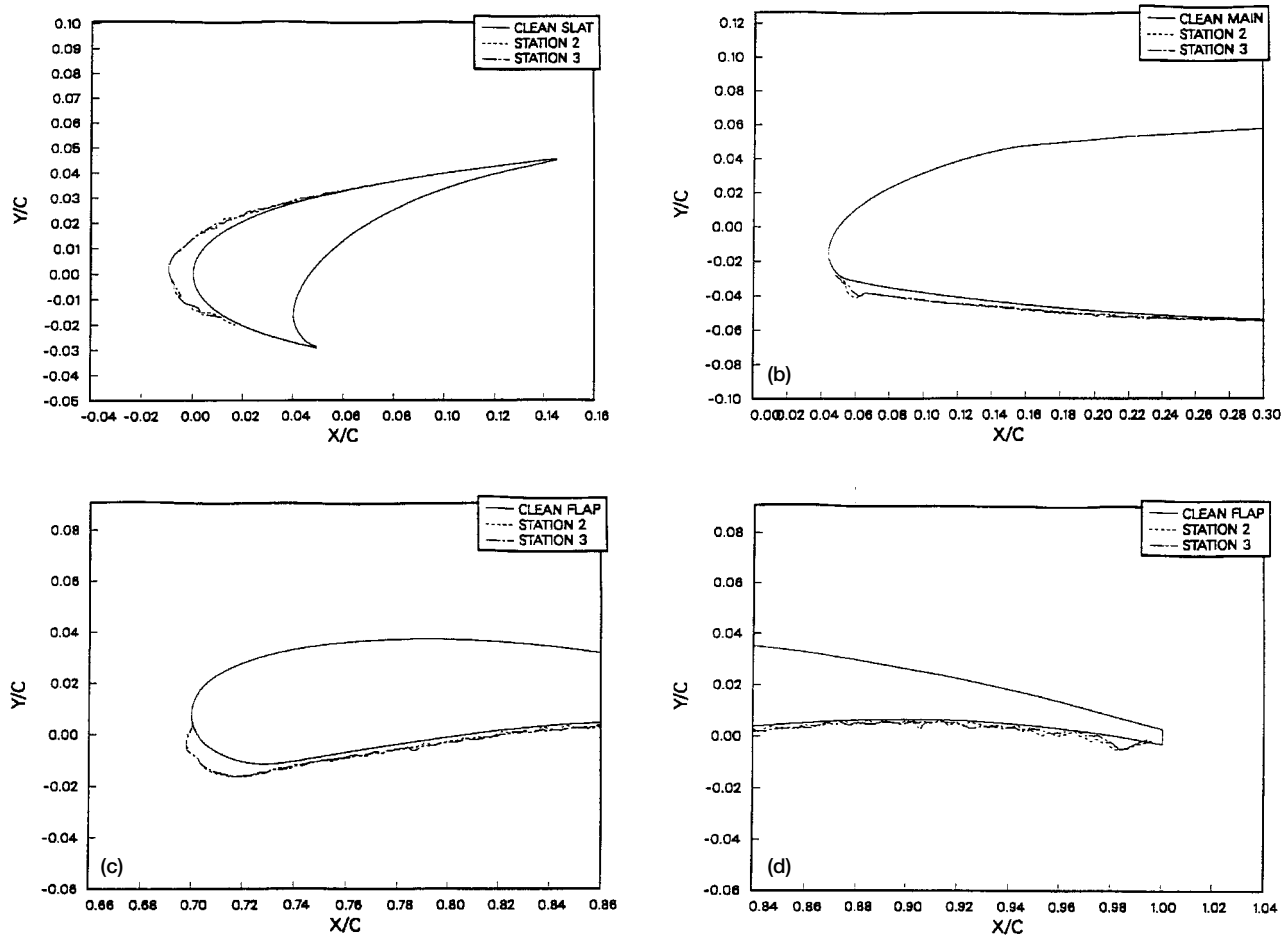

Figure 14.—Ice accretion traces for run number 41. AOA = 4°, T_t = 17 °F, V = 198 mph, LWC = 0.6 g/m^3, MVD = 20 μm, t = 6 min. (a) Slat. (b) Main element. (c) Flap leading edge. (d) Flap trailing edge.

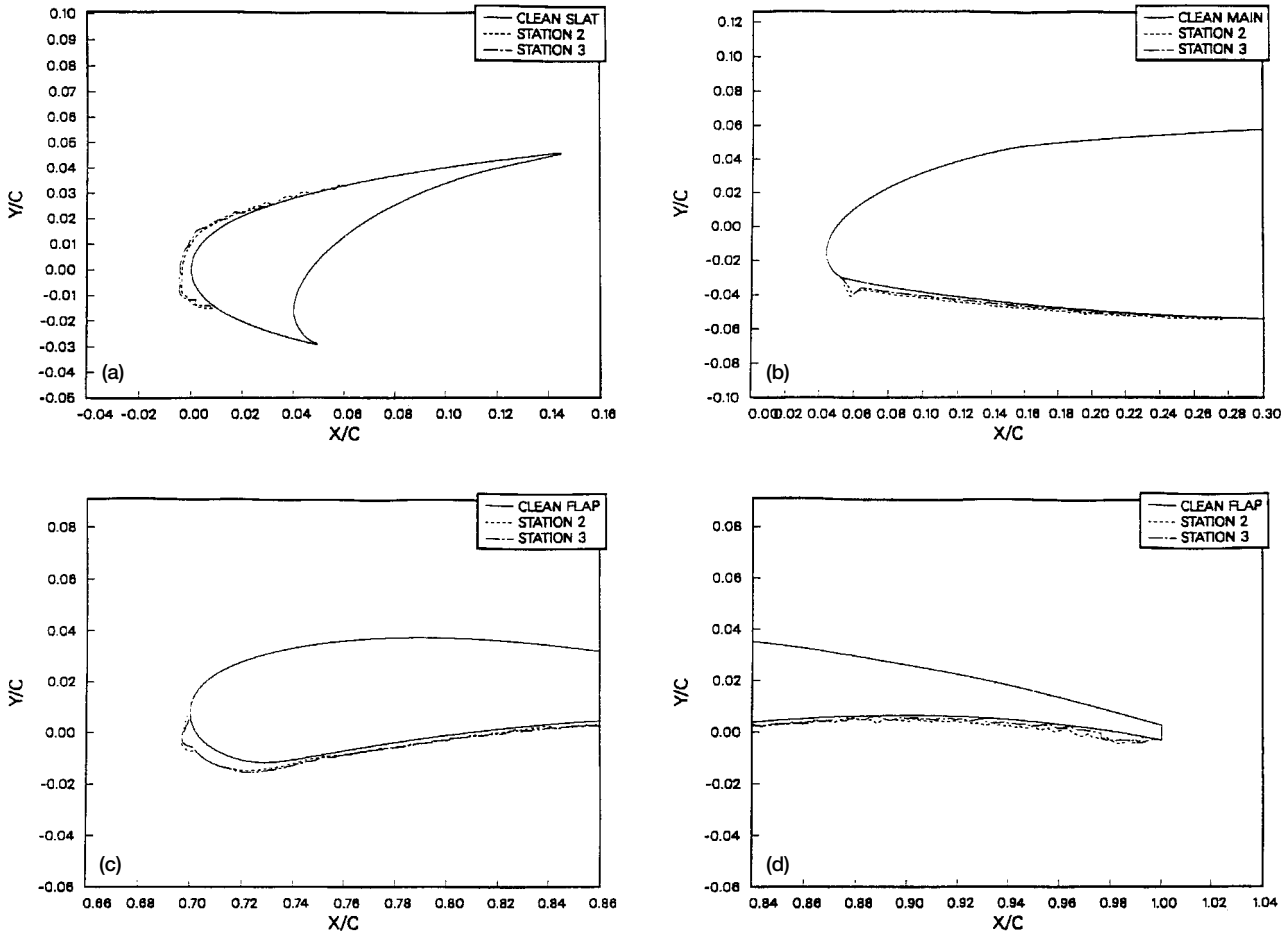

Figure 15.—Ice accretion traces for run number 39. AOA = 4°, T_t = 27 °F, V = 150 mph, LWC = 0.6 g/m^3, MVD = 20 μm, t = 6 min. (a) Slat. (b) Main element. (c) Flap leading edge. (d) Flap trailing edge.

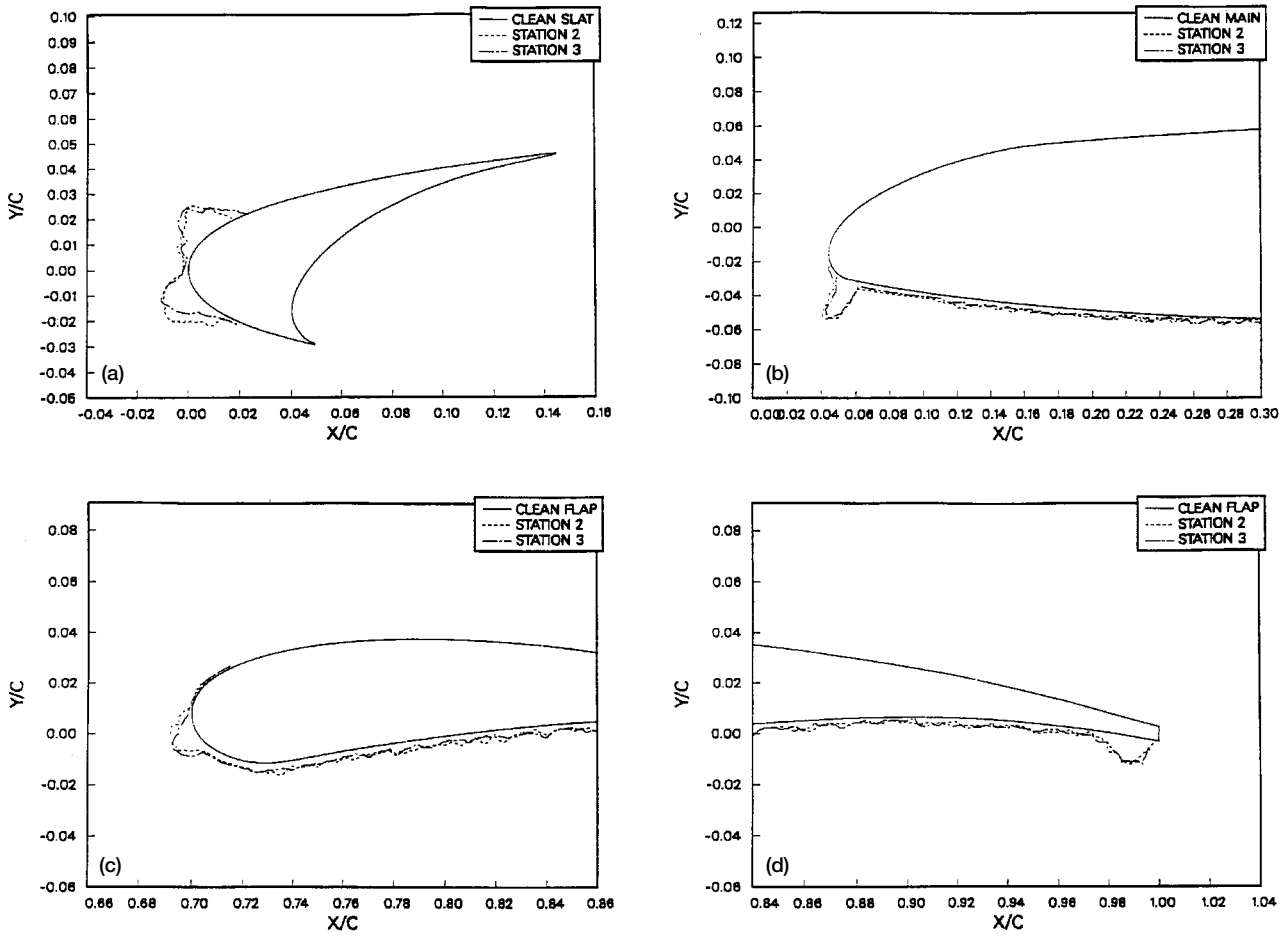

Figure 16.—Ice accretion traces for run number 107. AOA = 4°, T_t = 30 °F, V = 198 mph, LWC = 1.2 g/m^3, MVD = 20 μm, t = 6 min. (a) Slat. (b) Main element. (c) Flap leading edge. (d) Flap trailing edge.

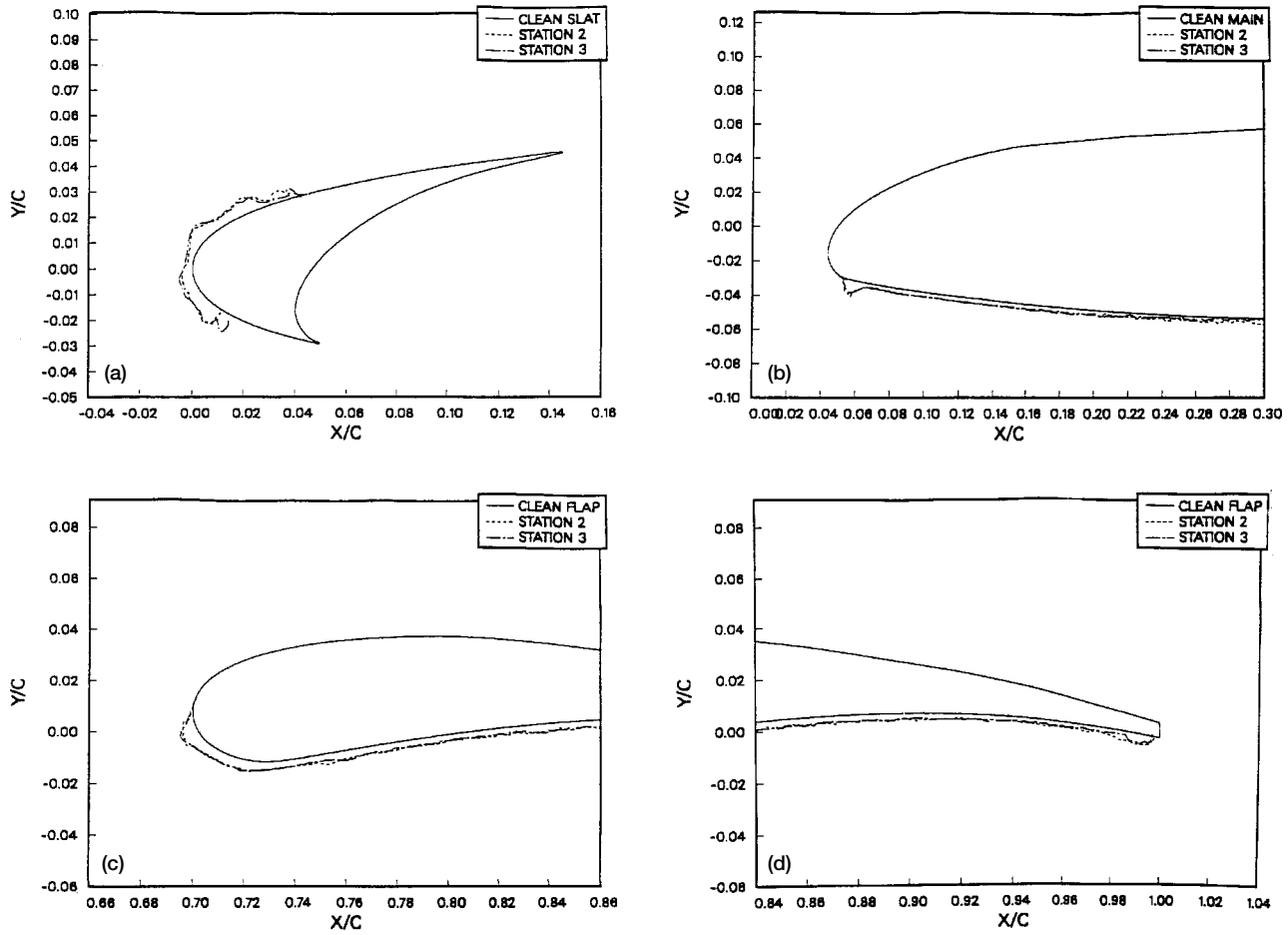

Figure 17.—Ice accretion traces for run number 34. AOA = 4°, T_t = 30 °F, V = 198 mph, LWC = 0.6 g/m^3, MVD = 25 μm, t = 6 min. (a) Slat. (b) Main element. (c) Flap leading edge. (d) Flap trailing edge.

REPORT DOCUMENTATION PAGE

Form Approved
OMB No. 0704-0188

1. AGENCY USE ONLY (*Leave blank*)	2. REPORT DATE	3. REPORT TYPE AND DATES COVERED
	June 1994	Technical Memorandum

4. TITLE AND SUBTITLE

Icing Test Results on an Advanced Two-Dimensional High-Lift Multi-Element Airfoil

5. FUNDING NUMBERS

WU–505–68–10

6. AUTHOR(S)

Jaiwon Shin, Peter Wilcox, Vincent Chin, and David Sheldon

7. PERFORMING ORGANIZATION NAME(S) AND ADDRESS(ES)

National Aeronautics and Space Administration
Lewis Research Center
Cleveland, Ohio 44135–3191

8. PERFORMING ORGANIZATION REPORT NUMBER

E–8906

9. SPONSORING/MONITORING AGENCY NAME(S) AND ADDRESS(ES)

National Aeronautics and Space Administration
Washington, D.C. 20546–0001

10. SPONSORING/MONITORING AGENCY REPORT NUMBER

NASA TM–106620
AIAA–94–1869

11. SUPPLEMENTARY NOTES

Prepared for the 12th Applied Aerodynamics Conference sponsored by the American Institute of Aeronautics and Astronautics, Colorado Springs, Colorado, June 20–22, 1994. Jaiwon Shin and David Sheldon, NASA Lewis Research Center; Peter Wilcox and Vincent Chin, McDonnell Douglas Aerospace, Long Beach, California 90846. Responsible person, Jaiwon Shin, organization code 2720, (216) 433–8714.

12a. DISTRIBUTION/AVAILABILITY STATEMENT

Unclassified - Unlimited
Subject Category 02

12b. DISTRIBUTION CODE

13. ABSTRACT ***(Maximum 200 words)***

An experimental study has been conducted to investigate ice accretions on a high-lift, multi-element airfoil in the Icing Research Tunnel at the NASA Lewis Research Center. The airfoil is representative of an advanced transport wing design. The experimental work was conducted as part of a cooperative program between McDonnell Douglas Aerospace and the NASA Lewis Research Center to improve current understanding of ice accretion characteristics on the multi-element airfoil. The experimental effort also provided ice shapes for future aerodynamic tests at flight Reynolds numbers to ascertain high-lift performance effects. Ice shapes documented for a landing configuration over a variety of icing conditions are presented along with analyses.

14. SUBJECT TERMS

High-lift; Multi-element airfoil ice accretion

15. NUMBER OF PAGES

22

16. PRICE CODE

A03

17. SECURITY CLASSIFICATION OF REPORT	18. SECURITY CLASSIFICATION OF THIS PAGE	19. SECURITY CLASSIFICATION OF ABSTRACT	20. LIMITATION OF ABSTRACT
Unclassified	Unclassified	Unclassified	